Colloid Polym Sci 279:1097–1103 (2001)

ORIGINAL CONTRIBUTION

G. Lagaly
O. Mecking
D. Penner

Colloidal magnesium aluminum hydroxide and heterocoagulation with a clay mineral. II. Heterocoagulation with sodium montmorillonite

Received: 28 February 2001
Accepted: 8 March 2001

G. Lagaly (✉)
Universität Kiel, Institut für Anorganische Chemie, 24098 Kiel, Germany
e-mail: h.mittag@email.uni-kiel.de

O. Mecking
Thüringisches Landesamt für Denkmalpflege, Abteilung Archäometrie
Humboldtstrasse 11
99443 Weimar, Germany

D. Penner
Forschungsinstitut für anorganische Werkstoffe–Glas/Keramik–GmbH
Heinrich-Meister-Strasse
56203 Höhr-Grenzhausen, Germany

Abstract Montmorillonite dispersions were completely coagulated by magnesium aluminum hydroxide when the hydroxide mass fraction, χ, was 0.2 or greater. The hydroxide dispersion required only a montmorillonite mass fraction of 0.06 for total coagulation. Thus, heterocoagulates were formed for $0.2 < \chi < 0.94$. At an excess of montmorillonite, network formation between the oppositely charged particles led to maxima of the yield value and the storage modulus at $0.4 < \chi < 0.5$. At higher hydroxide contents, $\chi > 0.5$, both properties decreased steeply, indicating the reduced mechanical stability of the network. Divalent anions at concentrations above 1 mmol/l acted as liquefying agents for the dispersed heterocoagulates. The specific surface area of the freeze-dried dispersions increased to a maximum value at $\chi = 0.65$. The pore size distributions revealed that montmorillonite lamellae and hydroxide particles were not homogeneously distributed.

Key words Gas adsorption · Heterocoagulation · Layered double hydroxide · Magnesium aluminum hydroxide · Montmorillonite

Introduction

The aggregation of colloidal particles responds to the state of stabilization in the dispersion and is very important in many practical applications. For instance, conditions must be chosen so that a sediment is easy to stir, a filter cake is permeable, or a drilling fluid obtains the required plastering effect [1].

A great variety of sediments are formed by anisometric particles [1–5]. The formation of different types of aggregates and sediments plays a decisive role in the practical application of millions of tons of clays [1, 6]. The Na^+/Ca^{2+} ratio is an important factor which determines aggregation and sedimentation behavior of clays and clay minerals. A further way to tune these properties could be heterocoagulation of the clay minerals with the "antitype", the layered double hydroxides, also called "anionic clays". An interesting application of montmorillonite–hydroxide mixtures was recently described. The combination of two layered materials with opposite layer charge signs provided an excellent solid stabilizer of oil/water emulsions [7, 8]. Envelopes of montmorillonite and hydroxide particles around and network structures between the oil droplets were made visible by X-ray microscopy [9, 10].

Materials and methods

Montmorillonite

Sodium montmorillonite was separated from Wyoming bentonite (Greenbond, our sample number 40A) by size fractionation (less than 2 μm) [11, 12]. The total cation-exchange capacity, $c_t = 1.03$ mEq/g sodium montmorillonite, and the layer charge, $\xi = 0.28$ Eq/mol, were measured by alkylammonium exchange [13]. The layer charge of 0.28 Eq/mol corresponds to an interlayer exchange capacity of $c_i = 0.74$ mEq/g sodium montmorillonite.

Magnesium aluminum hydroxide

Colloidal magnesium aluminum hydroxide was prepared as described in Ref. [14]. The colloidal material was obtained by peptization of the parent material aged at 0 °C (MAH-0), 20 °C (MAH-20), and 90 °C (MAH-90). Sample MAH-20 was used if not otherwise indicated.

Heterocoagulation

To determine the amount of hydroxide needed to coagulate a montmorillonite dispersion or vice versa, increasing volumes (in microliter steps) of a 2% hydroxide dispersion were added to 5 ml 2% montmorillonite dispersion and then diluted with water to give a total volume of 10 ml. After shaking for 24 h the dispersion was centrifuged (2000 rpm = 380*g*, Heraeus Biofuge). The presence or absence of colloidal material in the supernatant was tested with a laser beam. The 2% hydroxide dispersion was coagulated with a 0.2% sodium montmorillonite dispersion.

In the heterocoagulation experiments, the sodium montmorillonite dispersions were added to the hydroxide dispersions. When heterocoagulation was performed in the presence of salts, the hydroxide was mixed with the salt solution before the montmorillonite dispersion was added 10 min later. The hydroxide/montmorillonite ratio is expressed by the mass fraction of the hydroxide: χ = amount of hydroxide (g)/amount of hydroxide + montmorillonite (g). The total solid content of the mixed dispersions was varied between $\sigma = 0.5\%$ (w/w) and $\sigma = 4\%$ (w/w). Dispersions with higher solid and montmorillonite contents became gel-like.

The sediment height of the hydroxide–montmorillonite dispersions was measured more than 6 weeks after mixing (glass tubes, diameter 1 cm, height 17 cm).

The rate of heterocoagulation, $(dD/dt)_{t\to 0}$, was determined by measuring the increase in the optical density, D, of the 0.5% hydroxide dispersion after addition of different amounts of the 0.5% montmorillonite dispersion. After a short but intensive mixing (accomplished by withdrawing and reinjection of the dispersion) the increase in the optical density (extinction), $D = \log I_0/I$, was measured within the first minutes at a wavelength of 660 nm. We used a self-made multichannel photometer which recorded 512 extinction values within 5 s.

Electrophoretic mobility and rheological measurements

The electrophoretic mobility of the hydroxide–montmorillonite particles was measured by microelectrophoresis (PenKem 501). The flow behavior was studied with a Physica UDS 200 rotational viscometer with cone–plate geometry [14].

Gas adsorption

The specific surface area and the pore size distribution were determined by nitrogen adsorption at 77 K (Sorptomat Carlo Erba and a self-made gas adsorption instrument [15]). The mesopore size distribution was evaluated from the desorption branch on the basis of the slit-shaped geometry [16]. The specific mesopore surface area was calculated from the radii and the corresponding volume increments [16, 17]. From the t plots the number of micropores was zero or very small [18]. The samples studied by gas adsorption were obtained by freeze-drying the dispersions.

Results

Heterocoagulation

When 1.25 ml 1% magnesium aluminum hydroxide dispersion was added to 10 ml 1% sodium montmorillonite dispersion, all the colloidal particles were coagulated. This ratio corresponded to a hydroxide mass fraction $\chi = 0.2$ or a hydroxide/montmorillonite mass ratio 0.25:1. For $\chi < 0.2$ montmorillonite particles remained dispersed. To coagulate 10 ml 1% hydroxide dispersion, 3 ml 0.2% montmorillonite dispersion was required, corresponding to $\chi = 0.94$ or a hydroxide/montmorillonite mass ratio of 16.7:1. Thus, much smaller amounts of montmorillonite were needed to coagulate the hydroxide dispersion than hydroxide to coagulate the montmorillonite dispersion.

The sediment height, h, of the hydroxide–montmorillonite dispersions increased with the hydroxide content very steeply, reached a high value at the beginning of total coagulation at $\chi \sim 0.2$ and decreased at $\chi > 0.9$ (Fig. 1). Thus, voluminous sediments formed in the domain of total coagulation ($0.2 \le \chi \le 0.94$).

The particles coagulated slowly when small amounts of hydroxide were added (Fig. 2). The rate of coagulation increased with χ to a maximum at $\chi \sim 0.5$. Slightly higher amounts of hydroxide reduced the rate of coagulation steeply. The scattering of the data (±10% between parallel measurements) was caused by the difficulty to obtain a homogeneous distribution of particles immediately after mixing the dispersions.

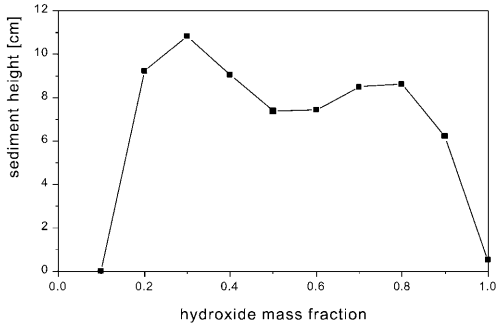

Fig. 1 Sediment height of montmorillonite/hydroxide dispersions. χ is the mass fraction of hydroxide. Solid content 1% (w/w)

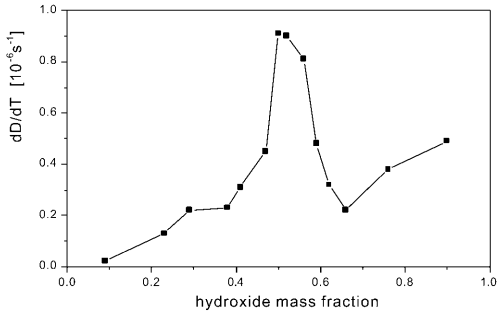

Fig. 2 The rate of heterocoagulation of hydroxide dispersions with montmorillonite, expressed by the increase in the optical density, (dD/dt), at $t \to 0$

Electrophoretic mobility

The mobility of the particles decreased linearly when hydroxide particles were added to the montmorillonite dispersion (Fig. 3). Direct visualization of the particle movement in the PenKem instrument clearly revealed that the particles became immobilized. At an excess of hydroxide ($\chi \geq 0.8$) the particles began to move again in the electric field, now in the opposite direction, and the mobility increased with the increasing hydroxide/montmorillonite ratio.

Rheological studies

A 2% hydroxide dispersion (MAH-20) showed a viscosity of 1.5 mPas and a yield value below 100 mPa. The yield value of the 2% sodium montmorillonite dispersion (Wyoming, M40A) was 430 mPa. The heterocoagulate dispersions ($\chi = 0.5$) showed distinctly higher values. The yield value of the three samples increased in a similar way (Fig. 4a) but the viscosity increase of MAH-90 was modest in comparison with MAH-0 and MAH-20 (Fig. 4b). The dispersions revealed viscoelastic behavior at solid contents, σ, above 1.5% (w/w). The storage modulus increased to 770 Pa (MAH-0), 812 Pa (MAH-20), and 590 Pa (MAH-90) at $\sigma = 3.5\%$ (w/w) (Fig. 4c). The loss modulus reached values between 40 and 95 Pa.

The yield value and viscosity as a function of the hydroxide mass fraction, χ, were small at high contents of montmorillonite ($\chi < 0.2$) and hydroxide ($\chi < 0.6$) (Fig. 5). With increasing hydroxide content the yield value rose to a maximum which shifted from $\chi = 0.35$ at $\sigma = 2\%$ to $\chi = 0.44$ at $\sigma = 3$ and 4%. The yield value decreased steeply at higher hydroxide contents. The viscosity increased to a maximum at $\chi \sim 0.4$ (40, 100, and 150 mPas at $\sigma = 2$, 3, and 4%). The storage and loss moduli revealed sharp maxima at the same composition (Fig. 6).

The flow curves included a hysteresis loop at mass contents of 2% (w/w) and higher and $0.2 < \chi < 0.6$. The behavior was antithixotropic with maximum hysteresis at $\chi \sim 0.4$. The flow of the 4% dispersion changed into weakly thixotropic behavior at $0.4 < \chi < 0.55$.

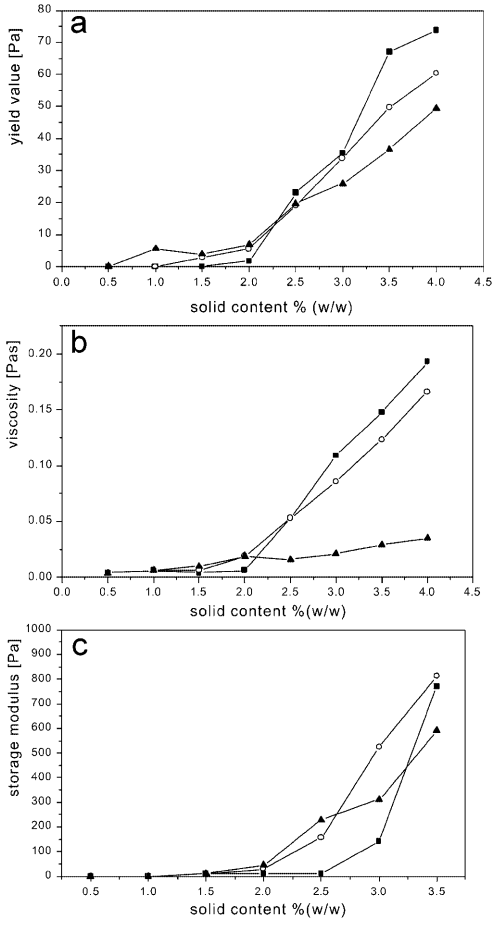

Fig. 4 **a** Yield value, **b** (plastic) viscosity, and **c** storage modulus of montmorillonite–hydroxide dispersions, $\chi = 0.5$, as a function of the solid content. Hydroxide MAH-0 (■), MAH-20 (⊙), MAH-90 (◆)

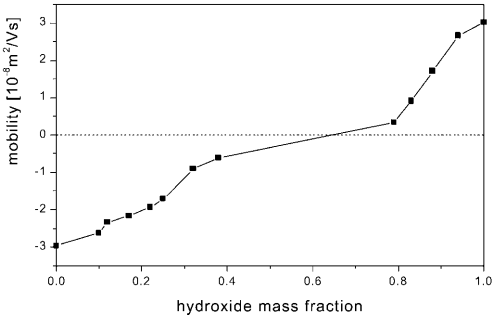

Fig. 3 Mobility of the montmorillonite–hydroxide particles. Solid content 0.06% (w/w). The particles were immobile between $\chi = 0.4$ and $\chi = 0.8$

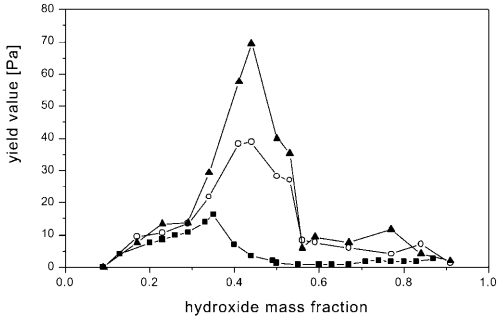

Fig. 5 Yield value of heterocoagulate dispersions with 2% (■), 3% (⊙), and 4% (◆) solid contents as a function of the hydroxide mass fraction

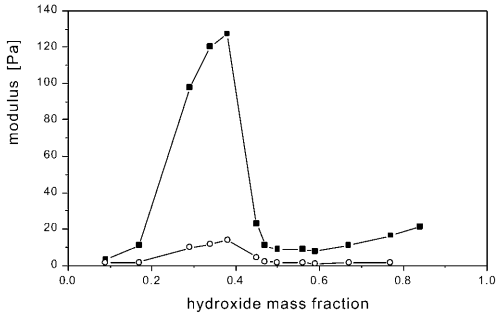

Fig. 6 Storage (■) and loss (⊙) moduli of 2% heterocoagulate dispersions as a function of the hydroxide mass fraction

Very small numbers of phosphate ions increased the yield value of the sodium montmorillonite dispersions (Table 1, $\chi = 0$). Concentrations higher than about 1 mmol/l reduced the viscosity and the yield value. Very high concentrations (above 1000 mmol/l) increased these values again [19, 20]. A first increase in the viscosity and the yield value followed by the liquefying effect was also observed for the dispersed heterocoagulates. Similar behavior was noticed when sodium carbonate was present. However, a liquefying effect was not observed for the pure hydroxide dispersion, $\chi = 1$ (Fig. 4b in Ref. [14]).

Specific surface area and porosity

The nitrogen adsorption isotherm of the montmorillonite with a pronounced hysteresis (Fig. 7a) is typical of these clay minerals [18, 21, 22] and is classified as a type IIb isotherm [23]. The specific surface area was 19.8 m^2/g (adsorption branch) and the mesopore volume was 15 μl/g. The pore size distribution showed a sharp peak at 1.2 nm (Fig. 8a). Such sharp peaks at small radii, however, may not represent the true pore size distribution.

The adsorption isotherm of the hydroxide was of type IV with a H_2-type hysteresis (Fig. 7b) [23]. The plateau at $p/p_0 \gtrsim 0.9$ was not very pronounced. The desorption branch approached asymptotically the adsorption branch at low pressures. Similar isotherms were measured, for instance, on mesoporous silica [23]. The magnesium aluminum hydroxide was mesoporous with a complicated crownlike pore size distribution (Fig. 8d). The specific surface area was mainly determined by the mesoporous surface area (Table 2).

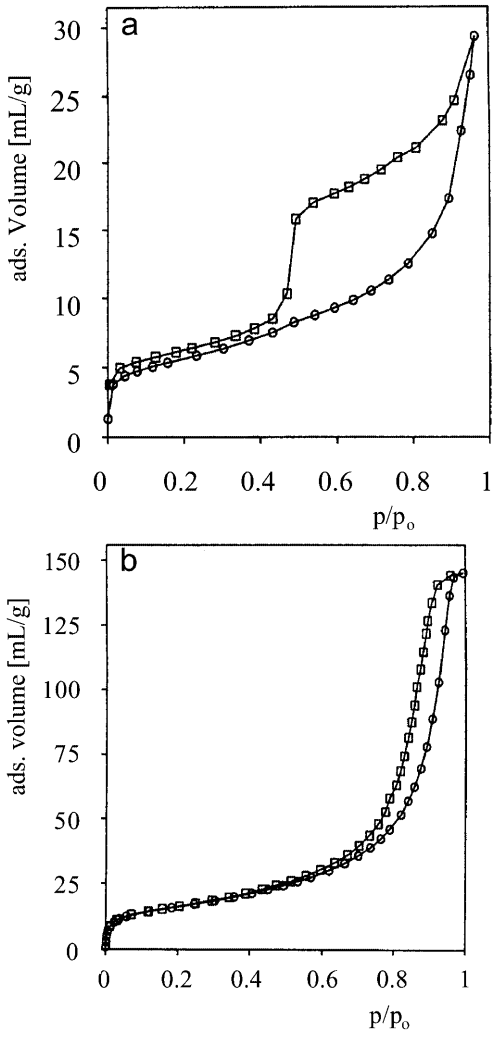

Fig. 7 Nitrogen adsorption and desorption isotherm (77 K) of **a** freeze-dried sodium montmorillonite and **b** magnesium aluminum hydroxide

Table 1 Yield value of 2% montmorillonite–hydroxide dispersions in the presence of Na_2HPO_4 and Na_2CO_3

Salt concentration (mmol/l)	Yield value (Pa)				
	$\chi = 0$[a]	$\chi = 0.3$[a]	$\chi = 0.5$[a]	$\chi = 1$[a]	$\chi = 0.5$[b]
0	0.4	17.2	0.4	0.1	0.4
0.1	2.2	> 30	8.7	0.1	0.9
0.5	2.0	24.0	6.1		10.7
1	2.0	9.4	4.0	0.8	7.0
10	1.0	3.0	0.5	1.2[c]	3.5
100	1.3		0.6	0.6	0.6

[a] Na_2HPO_4
[b] Na_2CO_3
[c] Maximum value of 3.0 Pa at 5 mmol/l

The surface area of the heterocoagulates increased to a maximum of about 100 m^2/g at $\chi = 0.65$, which corresponded to the maximum of the mesopore volume. The pore size distribution for the heterocoagulates (Fig. 8b, c, Table 2) was composed of the patterns of montmorillonite and hydroxide; however, increasing montmorillonite content shifted the maximum of the distribution attributed to the hydroxide to somewhat smaller pore sizes. The total specific surface area was

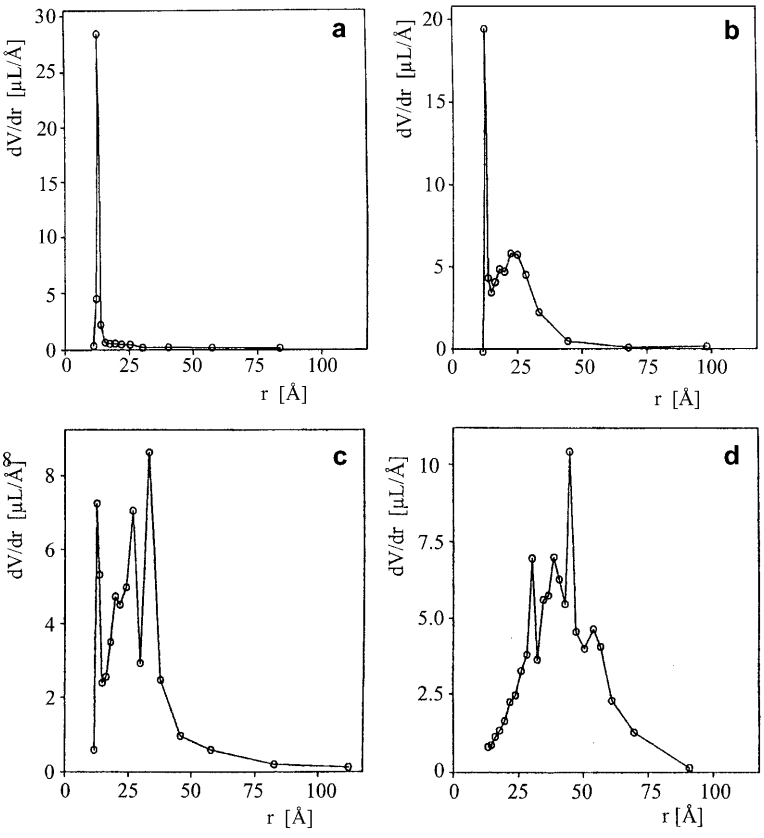

Fig. 8 Pore size distribution of freeze-dried montmorillonite/hydroxide heterocoagulates [17]: **a** sodium montmorillonite, $\chi = 0$; **b** $\chi = 0.35$; **c** $\chi = 0.5$; **d** hydroxide, $\chi = 1$

mainly determined by the mesopore surface area. (That the total specific surface area was smaller than the mesopore surface area was a consequence of the use of an idealized pore structure model in the calculations.)

The strong influence of the salts on the heterocoagulation was also evident from the pore size distribution (Fig. 9). The distribution curves for heterocoagulates ($\chi = 0.5$) prepared in the presence of 100 mmol/l Na_2CO_3 (similar Na_2SO_4) and 100 mmol/l Na_2HPO_4 showed a maximum at pore radii of 5–6 nm and were totally different from the curves in the absence of salt (Fig. 8c).

Table 2 Specific surface area and mesopore volume of heterocoagulates (freeze-dried dispersions with 1% solid content) [17]

χ	Specific surface area (m^2/g)		Mesopore volume (μl/g)	Mesopore surface area (m^2/g)
	Adsorption[a]	Desorption[a]		
0	19.8	21.2	15.0	6.2
0.2	21.7	21.8	75.0	32.7
0.35	29.4	28.8	104.2	43.8
0.5	55.5	54.5	142.0	49.5
0.65	99.6	101.1	264.0	95.2
0.8	41.3	42.1	164.1	53.6
1.0	57.6	58.3	218.0	57.9

[a] From the adsorption and desorption branch of the isotherm

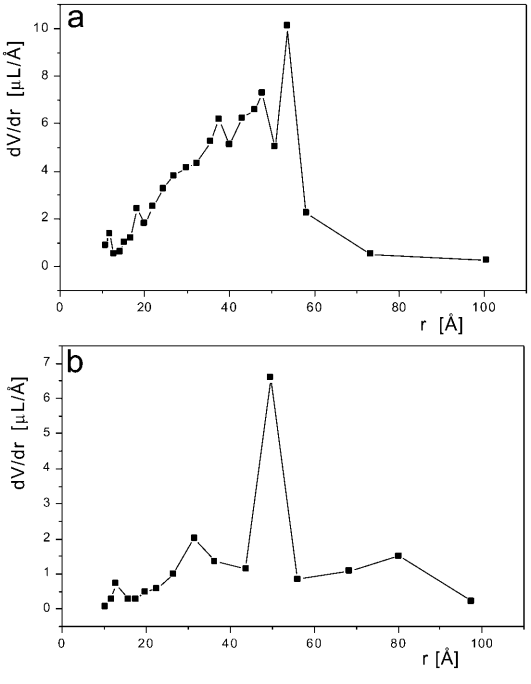

Fig. 9 Pore size distribution of samples prepared by addition of montmorillonite to the hydroxide dispersed in **a** 100 mmol/l Na_2CO_3 and **b** 100 mmol/l Na_2HPO_4. $\chi = 0.5$, solid content of the mixed dispersion 1% (w/w), dried at 70 °C

Discussion

Sodium montmorillonite delaminates into single silicate layers when dispersed in water [1, 6, 24]. As double hydroxides do not show this behavior, the thin, flexible montmorillonite layers could cover the hydroxide particles in a similar way as silicate layers coat the quartz grains in clay-bonded molding sands (cf. Fig. 3.28 in Ref. 6) [25, 26]. However, the montmorillonite layers of delaminated particles reaggregate very easily forming more or less thick lamellae. A modest concentration of magnesium and aluminum ions liberated from the magnesium aluminum hydroxide may be enough to initiate reaggregation of the silicate layers during heterocoagulation. The pore size distribution curves clearly indicate that at least a certain part of the silicate layers is aggregated. The X-ray powder diagrams also reveal aggregated silicate lamellae with coherent scattering domains. As indicted by the pore size distribution (Fig. 9), a higher degree of mixing of the hydroxide particles and montmorillonite lamellae was obtained in the presence of liquefying anions.

The distinctly larger diameter–thickness ratio of the montmorillonite lamellae is the reason why considerably smaller amounts of the clay mineral are required to coagulate the hydroxide dispersion than vice versa and why even small amounts of montmorillonite ($\chi = 0.9$) increase the sediment volume considerably (Fig. 1). Silicate lamellae span the distance between the hydroxide particles and form a network which leads to a large sediment volume. X-ray microscopy of Pickering emulsions made visible that the hydroxide particles and clay mineral lamellae build up a network within the coherent phase between the paraffin oil droplets [9, 10]. Modest numbers of multivalent anions liberated by the dissolved hydroxide promote the band-type aggregation of the clay mineral lamellae rather than the formation of distinct particles. This behavior is analogous to the effect of calcium ions. Small numbers of these cations create band-type networks and increase the yield value of sodium montmorillonite dispersions. Higher numbers promote aggregation to distinct particles and reduce the yield value and the viscosity [27].

The antithixotropic behavior at $0.2 < \chi < 0.45$ reveals that shearing moves the oppositely charged particles in positions of optimal network formation. As the mechanical stability of the networks is reduced at higher values of χ, time-dependent changes are no longer observed.

The sediment volume remains high between $\chi = 0.2$ and $\chi = 0.9$ (Fig. 1). The maximum at $\chi = 0.3$ is higher than at $\chi = 0.7$ because the montmorillonite lamellae with the large diameter/thickness ratio can span larger distances between the particles. The generally high sediment volume between $\chi = 0.2$ and 0.9 indicates that the ratio of the number of positive (hydroxide) and negative (montmorillonite) layer charges is not of primary influence. This also follows from the mobility measurements. The particles appeared to be totally immobilized between $\chi = 0.4$ and $\chi = 0.8$ (Fig. 3).

The maxima of the yield value (Fig. 5) lie in the range of χ where the particles appear to be immobilized. The rate of heterocoagulation (Fig. 2) also increases to a maximum at these hydroxide/montmorillonite ratios. The steep decrease in the yield value and the storage modulus at $\chi > 0.4$–0.5 indicates that networks containing a predominant number of hydroxide particles do not resist the mechanical stress as strongly as networks mainly consisting of clay mineral particles.

The ion-exchange capacity of the hydroxide and the montmorillonite is about 2.9 mEq/g and 1.03 mEq/g, respectively. A mixture of the composition $\chi = 0.26$ contains equal numbers of anionic and cationic layer charges.; however, the charges within the lamellae or particles do not contribute to the interparticle interactions or, in other words, would only contribute if both types of particles were fully delaminated. As the hydroxide particles do not disintegrate into single hydroxide layers [28], charge neutralization in relation to the external surfaces requires a higher number of hydroxide particles, i.e., a χ ratio somewhat higher than 0.26. The maxima of the yield stress and storage modulus at $\chi = 0.4$ may be considered as the condition of this charge neutralization.

The specific surface area (Table 2) does not change with χ in a similar way as the sediment volume. Owing to the mechanical stability of the three-dimensional network of particles at $\chi < 0.5$, freeze-drying yields a material with many macropores but fewer mesopores. In contrast, the network composed of hydroxide particles as the dominant component, $\chi > 0.5$, is more labile against mechanical stress. The freeze-dried material becomes denser (fewer macropores) but contains a higher number of mesopores, and the specific surface area and the mesopore volume show a maximum at the same hydroxide content, $\chi = 0.65$. When the yield value and the storage modulus are strongly reduced by liquefying anions, the network collapses and the specific surface, in the case of phosphate, decreases to 19 m^2/g. The effect of phosphate is strong because it acts as a liquefying agent for both the hydroxide and the clay mineral.

References

1. Lagaly G, Schulz O, Zimehl R (1997) Dispersionen und Emulsionen. Eine Einführung in die Kolloidik feinverteilter Stoffe einschließlich der Tonminerale – mit einem historischen Beitrag über Kolloidwissenschaftler von Klaus Beneke. Steinkopff, Darmstadt
2. Buining PA, Philipse AP, Lekkerkerker HNW (1994) Langmuir 10:2106–2114
3. Thies-Weesie DME, Philipse AP (1995) Langmuir 11:4180–4182
4. Thies-Weesie DME, Philipse AP, Kluijtmans SGJM (1995) J Colloid Interface Sci 174:211–223
5. Buitenhuis J, Philipse AP (1995) J Colloid Interface Sci 176:272–276
6. Jasmund K, Lagaly G (eds) (1993) Tonminerale und Tone. Struktur, Eigenschaften, Anwendung und Einsatz in Industrie und Umwelt. Steinkopff, Darmstadt
7. Abend S, Bonnke N, Gutschner U, Lagaly G (1998) Colloid Polym Sci 276:730–737
8. Abend S, Lagaly G (2001) Clay Minerals 36: in press
9. Thieme J, Abend S, Lagaly G (1999) Colloid Polym Sci 277:257–260
10. Neuhäusler U, Abend S, Jacobsen C, Lagaly G (1999) Colloid Polym Sci 277:719–726
11. (a) Tributh H, Lagaly G (1986) GIT Fachz Labor 30:524–529; (b) Tributh H, Lagaly G (1986) GIT Fachz Labor 30:771–776
12. Brandenburg U, Lagaly G (1988) Appl Clay Sci 3:263–279
13. Lagaly G (1994) In:Mermut A (ed) Charge characteristics of 2:1 clay minerals. CMS workshop lectures, vol 6. The Clay Minerals Society, Boulder, Colo, pp 1–46
14. Lagaly G, Mecking O, Penner D (2001) Colloid Polym Sci 279:1090–1096
15. Kruse HH, Beneke K, Lagaly G (1989) Colloid Polym Sci 267:844–852
16. Innes WB (1957) Anal Chem 29:1069–1073
17. Ewald W (1995) Thesis. Kiel University
18. Bojemueller E, Nennemann A, Lagaly G (2001) Appl Clay Sci 18:277–284
19. Abend S, Lagaly G (2000) Appl Clay Sci 16:201–227
20. Penner D, Lagaly G (2001) Appl Clay Sci 19:131–142
21. Barrer RM (1989) Pure Appl Chem 61:1903–1912
22. Cases JM, Berend I, Besson G, Francois M, Uriot JP, Thomas F, Poirier JE (1992) Langmuir 8:2730–2739
23. Rouquerol F, Rouquerol J, Sing K (1999) Adsorption by powders and porous solids. Academic, San Diego
24. Lagaly G (1989) Appl Clay Sci 4:105–123
25. Hofmann U (1961) Ber Dtsch Keram Ges 38:201–207
26. Hofmann U (1962) Keram Z 14:14–18
27. Permien T, Lagaly G (1994) Clay Miner 29:761–766
28. Albiston L, Franklin KR, Lee E, Smeulders JBAF (1996) J Mater Chem 6:871–877